Bio-Design and Manufacturing (2023) 6:136–149
https://doi.org/10.1007/s42242-022-00225-z

RESEARCH ARTICLE

Functionalized alginate-based bioinks for microscale electrohydrodynamic bioprinting of living tissue constructs with improved cellular spreading and alignment

Zhennan Qiu[1,2] · Hui Zhu[1,2] · Yutao Wang[1,2] · Ayiguli Kasimu[1,2] · Dichen Li[1,2] · Jiankang He[1,2]

Received: 20 July 2022 / Accepted: 24 November 2022 / Published online: 24 December 2022

Abstract

Bioprinting has been widely investigated for tissue engineering and regenerative medicine applications. However, it is still difficult to reconstruct the complex native cell arrangement due to the limited printing resolution of conventional bioprinting techniques such as extrusion- and inkjet-based printing. Recently, an electrohydrodynamic (EHD) bioprinting strategy was reported for the precise deposition of well-organized cell-laden constructs with microscale filament size, whereas few studies have been devoted to developing bioinks that can be applied for EHD bioprinting and simultaneously support cell spreading. This study describes functionalized alginate-based bioinks for microscale EHD bioprinting using peptide grafting and fibrin incorporation, which leads to high cell viability (>90%) and cell spreading. The printed filaments can be further refined to as small as 30 μm by incorporating polyoxyethylene and remained stable over one week when exposed to an aqueous environment. By utilizing the presented alginate-based bioinks, layer-specific cell alignment along the printing struts could be observed inside the EHD-printed microscale filaments, which allows fabricating living constructs with cell-scale filament resolution for guided cellular orientation.

Zhennan Qiu and Hui Zhu have contributed equally to this work.

✉ Jiankang He
jiankanghe@mail.xjtu.edu.cn

1 State Key Laboratory for Manufacturing Systems Engineering, Xi'an Jiaotong University, Xi'an 710049, China

2 NMPA Key Laboratory for Research and Evaluation of Additive Manufacturing Medical Devices, Xi'an Jiaotong University, Xi'an 710049, China

Graphic abstract

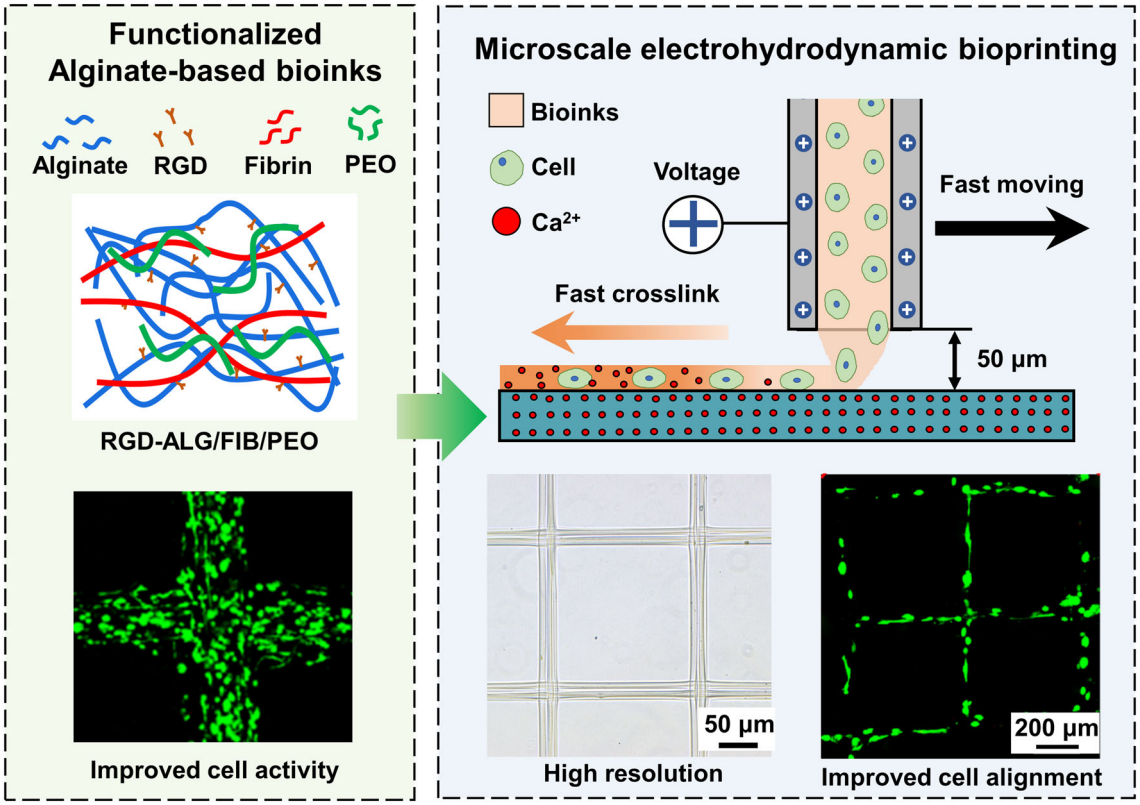

Keywords Microscale electrohydrodynamic bioprinting · Alginate-based bioinks · Cell spreading · Cell alignment

Introduction

Bioprinting is an advanced and emerging strategy for the controlled fabrication of living cellular constructs in vitro and in vivo, which exhibits great potential in biomedical fields such as tissue engineering, biomimetic tissue models, organ-on-a-chip systems, and regenerative medicine [1–3]. The commonly used cell printing techniques include inkjet- and extrusion-based or laser-assisted printing strategies [4–7]. However, these techniques cannot recapitulate real tissues at fine resolutions in three dimensions, which would hinder further mimicking the hierarchical structure and composition of the native extracellular matrix (ECM) [8–11]. For instance, skeletal muscle tissue is composed of densely packed and highly organized myofibers consisting of parallel multinucleated myotubes. Furthermore, muscle cell alignment plays an essential role in muscular tissue organization, contraction and maturation, as well as mechanical functions [12–14]. Therefore, many previous works have attempted to establish two-dimensional (2D) microgrooves, ridges and nanofibers to provide topological guidance for cell alignment in tissue engineering [15–18].

In recent years, electrohydrodynamic (EHD) printing has evolved as a novel strategy enabling the manufacture of high-resolution patterns and structures (100 nm–10 μm), which allows for the fabrication of fibers with smaller sizes than the extrusion nozzle diameter [19–24]. Particularly, a hydrogel bioink-based EHD bioprinting strategy was developed to fabricate well-organized living cell-laden structures [25–29]. In our previous work [25], living cellular constructs were EHD-printed at the microscale resolution (<100 μm) by using alginate solution as bioink, and the process parameters were optimized to reduce the side effect of high voltage on cell viability. However, the width of printed filaments ((82.4±14.3) μm) was still larger than the size of a single cell, and the encapsulated cells maintained spherical morphology in the EHD-printed constructs due to the inherent inert property of alginate bioink. In another research, Castilho et al. [30] investigated two kinds of photo-responsive hydrogel bioinks, namely gelatin and silk-based bioinks, for EHD bioprinting. Well-defined three-dimensional (3D) fiber constructs with small pores (down to 100 μm) and different geometries were successfully fabricated, in which the size of printed fiber

could be optimized in the range of 5–40 μm. However, the encapsulated cells showed relatively low viability with few cell spreading or alignment. Accordingly, it is still challenging for microscale EHD bioprinting to achieve well-aligned cellular constructs due to the lack of bioactive bioinks. Therefore, an urgent need persists for developing functionalized bioinks that are readily applicable for high-resolution EHD bioprinting to fabricate microscale cell-laden filaments and simultaneously support cellular spreading and alignment.

In this work, we aim to develop novel functionalized alginate-based bioinks for EHD bioprinting by grafting peptides and fibrin incorporation. The effect of bioink composition on printability as well as cell spreading and elongation is investigated. Polyoxyethylene (PEO) as an additive is further added to the functionalized bioinks to improve the bioprinting resolution. We expect that the developed alginate-based bioinks can effectively enhance cell spreading and precise deposition of the EHD-printed living structures for desired cell orientation.

Materials and methods

Materials

Alginate with medium viscosity was acquired from Sigma (UK). Lyophilized bovine blood plasma protein was bought from Millipore (USA). Lyophilized thrombin was purchased from Sigma-Aldrich (USA). 1-Ethyl-3-(3-dimethylaminopropyl) carbodiimide hydrochloride (EDC-HCl) was obtained from Aladdin (Tianjin, China). N-hydroxysulfosuccinimide sodium salt (sulfo-NHS) was obtained from Aladdin (Tianjin, China). 2-(N-morpholino)ethanesulfonic acid (MES) was obtained from Shanghai Yuanye Bio-Technology (Shanghai, China). The arginine–glycine–aspartic acid (RGD) peptide was purchased from Aladdin (Tianjin, China). Agarose powder with low melting temperature was purchased from Biowest (Spain). Calcium chloride powder was bought from Aladdin (Shanghai, China). The Cell Counting Kit-8 (CCK-8, MA0218) was purchased from Dalian Meilun Biotechnology Co., Ltd. (China).

Preparation of the functionalized alginate-based bioinks

Preparation of composite inks consisting of alginate and fibrin (ALG/FIB)

In this step, 3% (w/v) alginate solution was prepared by dissolving alginate powder into Dulbecco's Modified Eagle Medium (DMEM). 6% (w/v) fibrinogen solution was produced by dissolving lyophilized bovine blood plasma protein at 37 °C in sterile Dulbecco's phosphate-buffered saline (DPBS). The solution was kept at 37 °C for 45 min for adequate dissolution. The 3% (w/v) alginate solution was then mixed with 6% (w/v) fibrinogen solution in a volume ratio of 2:1 to obtain the composite solutions.

Formation of composite inks consisting of RGD-alginate, fibrin and PEO

The immobilization of RGD peptide to alginate was carried out by utilizing aqueous carbodiimide chemistry [31]. A typical conjugation reaction is described here for the preparation of alginate with 5% degree of substitution. Briefly, 1 g of alginate (5 mmol –COOH) was dissolved in 0.1 M MES buffer solution (0.3 M NaCl, pH 6.5) to form a 1% (w/w) solution. Then, 53.3 mg (0.25 mmol) sulfo-NHS and 47.9 mg (0.25 mmol) EDC-HCl were added. After 30 min, 86.6 mg (0.25 mmol) RGD dissolved in a minimum amount of MES buffer was dropped into the alginate solution, the pH was adjusted to 6.5–7.0, and the mixture was stirred overnight at room temperature. The RGD-alginate (RGD-ALG) was purified by dialysis against distilled water for 3 days using a 3500 molecular weight cut-off (MWCO) membrane and then lyophilized for 3 days. 3% (w/v) RGD-ALG solution was obtained by dissolving the above RGD-ALG into DMEM. Next, the RGD-ALG inks combining fibrin (RGD-ALG/FIB) were prepared by mixing 3% (w/v) RGD-alginate solution and 6% (w/v) fibrinogen solution in a volume ratio of 2:1. Finally, various weight fractions of PEO (1%–3% w/v) composite inks were prepared by mixing RGD-ALG/PEO solution and fibrinogen solution.

Characterization of the functionalized alginate-based bioinks

The chemical structure of synthesized copolymer was characterized by hydrogen nuclear magnetic resonance (^{1}H NMR) and Fourier transform infrared spectroscopy (FTIR). The NMR spectra were measured on a Bruker Avance-400 spectrometer, and 1 chemical shift (δ) was reported in ppm (1 ppm=1×10^{-6}). The ^{1}H NMR spectra were recorded at 400 MHz, 25 °C, with 32 scans, in NMR solvents (D_2O), and referenced internally to the corresponding solvent resonance. The FTIR spectrum was collected on a VERTEX 70v FT-IR spectrometer using the attenuated total reflectance (ATR) method and recorded in the 4000–650 cm range. The absorption maxima (ν max) were reported in wavenumbers (cm^{-1}).

The viscosities of various inks were tested using Kinexus pro + (Malvern, UK). An oscillatory strain sweep ranging from 0.01% to 100% with an oscillating frequency of 1 Hz was conducted to determine the linear viscoelastic region. Samples for these tests were measured at 25 °C and evaluated

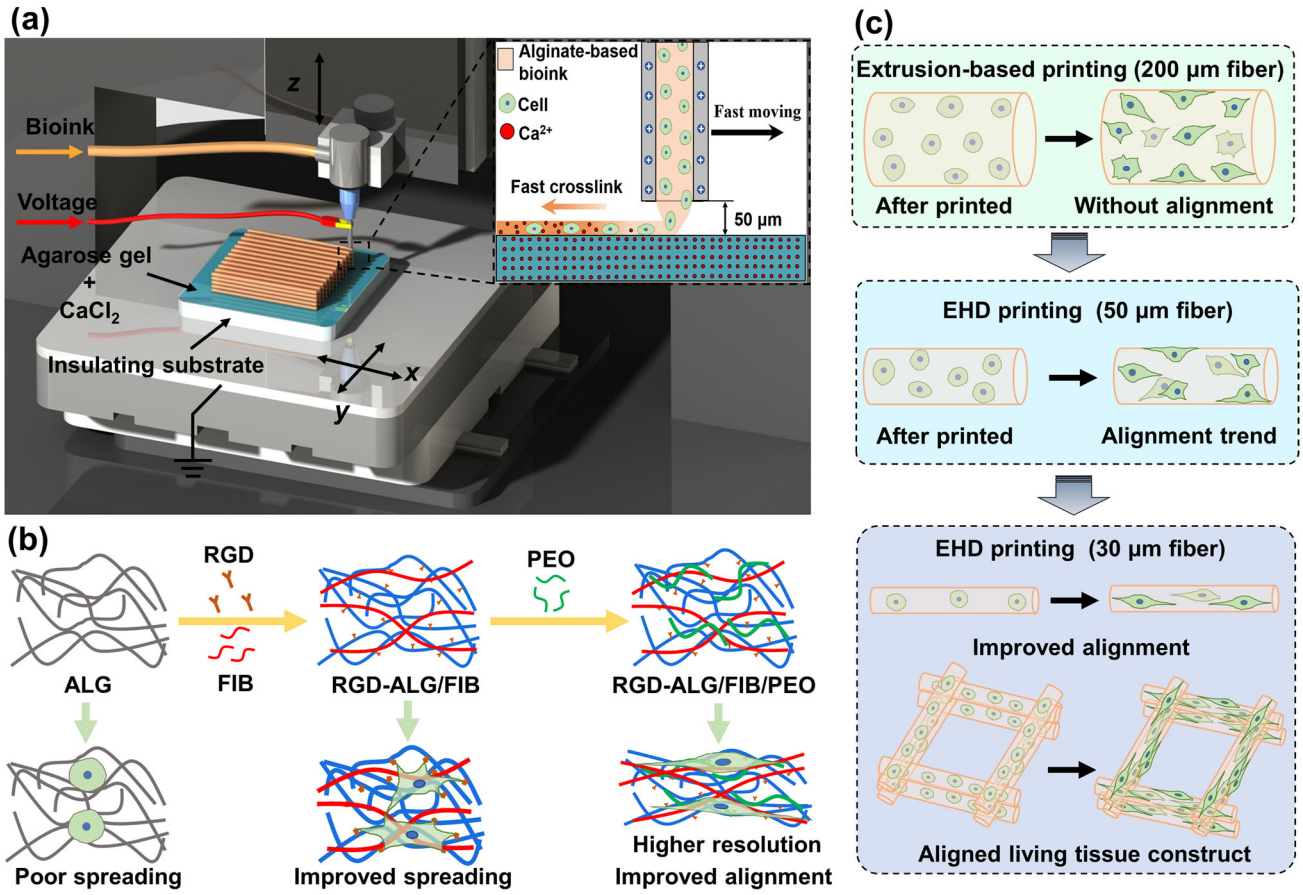

Fig. 1 Schematic of microscale electrohydrodynamic bioprinting living tissue constructs using functionalized alginate-based bioinks: **a** electrohydrodynamic bioprinting process; **b** development of alginate-based bioinks with improved cellular spreading and printing accuracy; **c** the cellular alignment improves with the decreasing filament width of alginate-based hydrogel

by increasing the shear rate from 0.1 to 100 s^{-1}. The surface tensions of solutions were determined by the platinum plate method using a tensiometer (QBZY, Fangrui, China). For the surface tension measurement, 6 mL of each solution was used for the analysis and the temperature was kept at 25 °C. All measurements were taken in three replicates.

Microscale EHD bioprinting of the functionalized alginate-based bioinks

Preparation of insulating substrate for EHD bioprinting

For this procedure, 2% (w/v) agarose solution was prepared by dissolving agarose and calcium chloride in deionized water at 100 °C. The concentration of calcium chloride in the agarose solution was 1% (w/v). Flat agarose hydrogel with a thickness of 2 mm was prepared by casting agarose solution in a Petri dish.

EHD printing of alginate-based bioinks and fiber diameter measurements

High-resolution bioactive constructs were fabricated in a home-made electrohydrodynamic printing platform shown in Fig. 1. To fabricate microscale hydrogel fibers, inks were loaded into 1-mL syringe which was controlled by the syringe pump. A printing nozzle was fixed on the *z*-axis and connected with the positive terminal of a high-voltage generator. Insulating Petri dish and agarose hydrogel with calcium ions were sequentially placed on the grounded *x*–*y* moving stage as the collecting substrate. The nozzle was connected with the syringe loaded with bioactive inks via a soft tube, as shown in Fig. 1. The process parameters such as feeding rate, applied voltage, nozzle-to-collector distance, and stage moving speed for EHD printing were fixed at 80 μL/h, 3 kV, 50 μm, and 65 mm/s, respectively. Alginate in the printed inks was instantly crosslinked in contact with agarose hydrogel composed of calcium ions to form hydrogel filaments and deposit onto the collecting substrate. The deposition of

hydrogel filaments could be flexibly controlled to fabricate complex patterns by directing the movement of *x*–*y* stage according to any user-specific design. When the printing process was finished, cross-linker solution was further dropped onto the surface of the hydrogel structure, which was then placed in a 37 °C thermostatic cell incubator for 15 min to obtain the fully crosslinked hydrogel structure.

Next, multilayer constructs with layer-specific orientations were fabricated in a layer-by-layer manner. In each layer, hydrogel microfibers were printed and stacked to form parallel microwalls while the wall spacing was kept at 250 μm. Five layers of hydrogel microwalls were fully printed to form bioactive constructs. The orientation of the microwalls from bottom to top was gradually changed from 0°, through 60° to 120°. The images were collected and analyzed by the region of interest (ROI) and measure functions in ImageJ. Six images were measured per printing condition, and 60 fiber measurements were taken per image. Histograms were generated and analyzed using Origin software.

Microscale EHD bioprinting of cell-laden constructs

For EHD bioprinting, agarose substrates and all other materials used for making inks were sterilized under ultraviolet (UV) light for 2 h before use. RGD-ALG/FIB/PEO solution was prepared as described in "Formation of composite inks consisting of RGD-alginate, fibrin and PEO" section followed by encapsulating C2C12 cells to form the bioinks with a cell density of 2×10^6 mL^{-1}. The EHD bioprinting process was in line with in "EHD printing of alginate-based bioinks and fiber diameter measurements" section under a sterilized environment. Then, the printed structures were washed with cell culture media and kept in an incubator at 37 °C under 99% CO_2, and the culture medium was changed every 2 days. For comparison, extrusion bioprinting was also performed by using pure alginate, ALG/FIB, RGD-ALG, and RGD-ALG/FIB inks encapsulating C2C12s crosslinked with 1% (w/v) calcium chloride solution and thrombin solution in a volume ratio of 19:1. The concentration of thrombin in the cross-linker solution was 10 units/mL. To further promote cell activity, a collagen layer was applied to cover the printed structures by using RGD-ALG/FIB/PEO bioink, and the structures were kept in an incubator and stained for F-actin and nuclei.

Characterizations of the EHD-printed constructs

The macro/microscopic images of the resultant constructs were viewed with a digital camera (Nikon, Japan) or an optical microscope. The diameter of printed filaments was statistically analyzed using at least three replicates. For testing the swelling ratio of the EHD-printed scaffolds, they were immersed into phosphate-buffered saline (PBS) solution and kept at 37 °C for up to 7 days. The diameter changes of the printed filaments were statistically analyzed by using three replicates.

Cell viability was quantified by performing CCK-8 and Live/Dead assay (Thermo Fisher Scientific); the cytoskeleton was stained with Alexa Fluor 594 phalloidin (Invitrogen), and cell nuclei were stained with DAPI according to the manufacturers' specifications. The florescence images of cells were captured using a super-resolution confocal microscope (A1, Nikon, Japan). All image processing and analysis were conducted using ImageJ (Available online: https://imagej.nih.gov/ij/) by modifying the brightness and contrast in bright field images to define the cell shape. Thereafter, cell spreading could be quantified and compared by measuring the cellular circularity ($4\pi\times$area/perimeter^2), which corresponds to a value of 1 for a perfect circle of at least 70 cells for each condition [32, 33]. To analyze the orientation of cells, we calculated the angle formed between the vector of the filament direction and the "orientation vector" given by the orientation of the main axis of each cell. The aligned cells were defined as ones with an absolute value of angle between 0° and 45° [34]. The angle calculation was performed automatically using ImageJ software.

Statistical analysis

All experiments were run in triplicate for each sample, and the quantified data were presented as mean±standard deviation. Statistical differences were analyzed by one-way ANOVA, and the significance was considered at the level of $^{*}p<0.05$, $^{**}p<0.01$.

Results and discussion

We firstly verified the success of RGD grafting on alginate and assessed the effect of ink compositions on their rheologic characteristics. The FTIR spectrum (Fig. 2a) shows the typical absorption bands of sodium alginate: mainly O–H stretching at 3424 cm^{-1}, pyranoid ring C–H stretching at 2963 and 2932 cm^{-1}, COO– symmetric and asymmetric stretching at 1611 cm^{-1} and at 1415 cm^{-1}, C–O–C stretching at 1094 cm^{-1}, and C–O stretching at 1338 and 1298 cm^{-1}. RGD was successfully conjugated onto alginate chains according to Fig. 2a where a peak appeared at 1281 cm^{-1} linked to the C–N stretch, which confirmed the formation of a stable peptide conjugation [35]. NMR spectroscopy was also adopted to confirm the RGD modification. As shown in Fig. 2b, the signals corresponding to the protons of the methylene groups of arginine and aspartic acid (2.20–2.90 ppm) appear in the spectra, indicating successful peptide grafting. The signals at 1.30 and 3.20 ppm correspond to low-molecular-weight by-products (N-acylurea) [36]. A

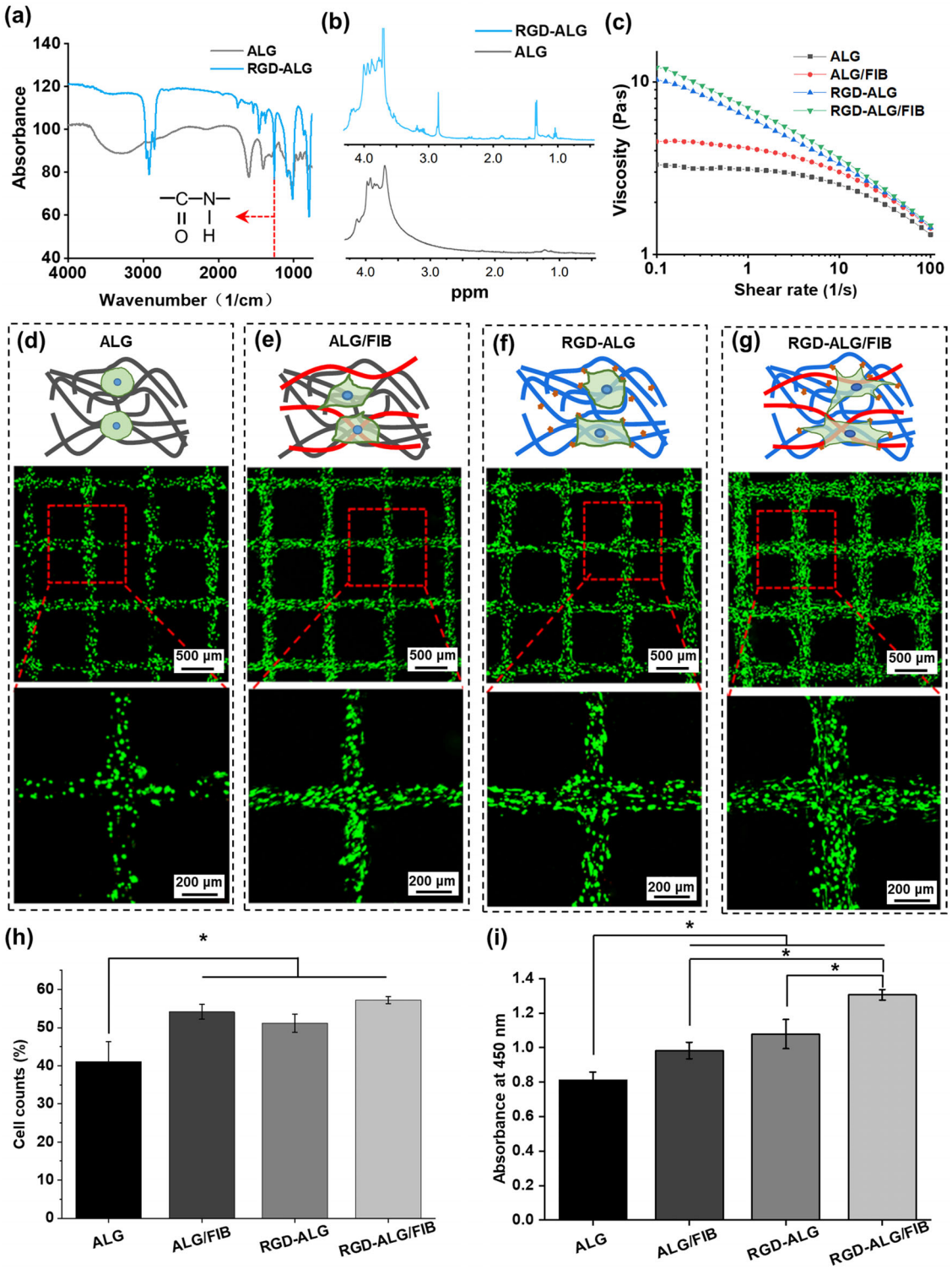

Fig. 2 **a** Fourier transform infrared spectroscopy (FTIR) and **b** hydrogen nuclear magnetic resonance (^{1}H NMR) spectra of pure alginate and arginine–glycine–aspartic acid (RGD)-modified alginate. **c** Viscosity changes of various alginate-based inks with increasing shear rate. **d**–**g** Fluorescent images of extrusion-based printing living tissue constructs with alginate hydrogel, alginate and fibrin (ALG/FIB) hydrogel, RGD-ALG hydrogel, and RGD-ALG/FIB hydrogel after culture for 1 day. **h** Cell counts with circularity smaller than 0.4 in different bioprinted constructs. **i** Cell Counting Kit-8 (CCK-8) tests of the extrusion-based printed C2C12s after 1 day of culture. All data are displayed as mean±standard deviation (SD). $^*p<0.05$, analyzed via one-way ANOVA. 1 ppm=1×10^{-6}

rheological test was carried out to investigate the printability of the various alginate-based inks. As shown in Fig. 2c, the viscosity of alginate increased considerably with the addition of RGD sequences, which could be a result of the crosslinking effect of between RGD peptides and alginate molecular chains [37]. The combination of fibrin would further increase the viscosities of both alginate and RGD-alginate, which indicated that the addition of fibrin promoted protein expansion and the interaction of polymer chains [38]. Besides, it should be noted that all the alginate-based hydrogels tested here exhibited shear thinning behavior that would be in favor of ink extrusion.

In order to verify the biocompatibility of the bioinks developed in this work, extrusion bioprinting was first adopted with four groups of bioinks encapsulated with C2C12 cells to form 10-layer cell-laden structures. After one day of culture, the live/dead staining images of cells were recorded and are shown in Figs. 2d–2g. The cells maintained high activity in all constructs; however, most of the cells in the pure alginate structure did not spread and showed spheroidal morphologies. Cell stretching could be improved significantly by either RGD modification or fibrin doping. Furthermore, cell circularity as a specific cell shape morphology descriptor was quantified according to its frequency distribution, and cells with circularity range of 0–0.4 were considered low-circularity cells, as shown in Fig. 2h [39]. The percentage of cellular circularity smaller than 0.4 was the highest in RGD-ALG/FIB ink among the four groups, reaching 57%, indicating that the RGD-ALG/FIB ink could boost fast cell spreading with more elongated morphology. This was in line with its fluorescence images showing fusiform cells with flourishing interactions. To further quantify and compare the cell performance of those bioinks, a CCK-8 test was carried out, and the results showed that RGD-ALG/FIB ink could keep the highest cell viability. As is well known, the RGD sequence is one of the most widely employed peptides to promote cell adhesion on a biomaterial because it has similar tripeptide motif corresponding to the essential cell adhesion peptide sequence identified in many ECM proteins [40, 41]. In this work, a stable covalent amide bond could be formed between the N-terminus of RGD peptides and the carboxyl group of the alginate to generate a cell-friendly 3D environment [42]. Moreover, the involvement of fibrin can further promote cell adhesion and spreading in the developed functionalized alginate-based bioinks due to its highly biocompatible nature.

The printing process parameters were subsequently optimized, as presented in Fig. 3. It was found that the printed line width increased from (51.6±4.3) to (101.6±3.2) μm with the feeding rate increasing from 200 to 300 μL/h (Fig. 3a), at a fixed moving speed of 45 mm/s and voltage of 3 kV. Besides, the printed line width decreased from (125.8±2.9) to (51.6±4.3) μm with the moving speed increasing from 35 to 45 mm/s (Fig. 3b), at a fixed feeding rate of 200 μL/h and voltage of 3 kV. These results indicated that the width of the EHD-printed fibers could be tuned independently by controlling the feeding rate of the inks and the moving speed of the substrate. A slower feeding rate of solution and a higher moving speed of the printing stage would lead to thinner fibers. To further improve the printing accuracy, PEO was involved in ink formulations because PEO additions were expected to prevent droplet formation, and thus allow for the formation of a steady jet. The effect of PEO concentration on the printing accuracy of RGD-ALG/FIB ink was investigated both as shown in Figs. 3c and 3d. With the PEO concentration increasing from 0 to 3%, the line width narrowed from (51.6±4.3) to (25.6±2.5) μm. By simply adding PEO to the ink solution, we could ensure precise patterning with precise control of the layer-by-layer nanofiber deposition, which is consistent with previous research on EHD printing and near-field electrospinning [30]. To clarify the internal mechanism of the impact of ink properties on the precise printing, the viscosities and surface tension of various inks with different PEO concentrations were tested. Figure 3e shows that the zero-shear viscosity increased with PEO concentration, which is agreement with previous observations on other polymer solutions due to the more drastic chain entanglement of long-chain PEO. This would help form uniform beadless fibers during the EHD process in this study, which may be due to the considerate threshold of polymer entanglement for electrohydrodynamic jet [43]. Interestingly, Fig. 3f shows that the addition of PEO could reduce the surface tension of inks; for example, the surface tension of the ink with 3% PEO decreased by 37% compared to that without PEO. The reduction in the surface tension with increasing PEO concentration has been reported in previous research, which was explained by the changing hydrogen bonding with water [44]. During the EHD printing process, the electrical stresses acting on the liquid surface will overcome the surface tension stress to make the liquid meniscus form a Taylor cone wherefrom a thin jet of ink is emitted [45]. As a result, decreasing the surface tension of inks can help the formation of Taylor cone and thus effectively reduce the width of the printed lines, leading to high-resolution 3D printing. In this study, the optimized experimental condition used PEO solution with 2 wt% to ensure the precise printing and the good biocompatibility of ink at the same time, despite the fast release of PEO from printed constructs after immersion in the cell culture medium [30]. As shown in Figs. 3g and 3h, 10- and 20-layer structures can be finely EHD-printed using RGD-ALG/FIB/PEO bioink. The line widths of 10- and 20-layer structures were (27.2±2.5) μm and (30.7±4.5) μm, respectively, which indicated that the multi-layer hydrogel structures could still be kept thin. Besides, the height of the 20-layer structures could reach to (41.8±3.5) μm.

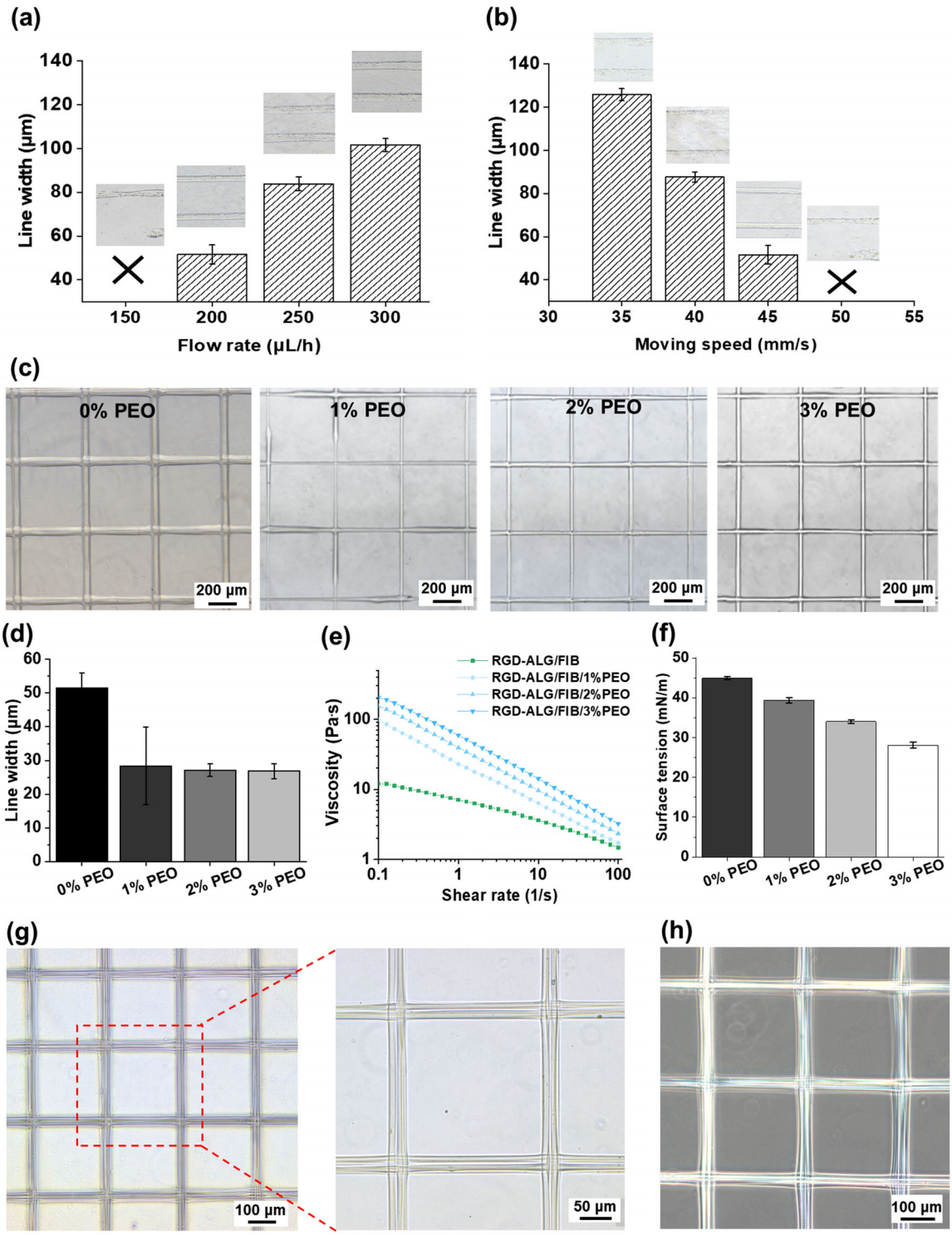

Fig. 3 **a**, **b** Effect of feeding rate and stage moving speed on the width of electrohydrodynamically printed filaments. **c** Light microscope images of electrohydrodynamic (EHD)-printed filaments by using different inks with increasing polyoxyethylene (PEO) concentrations. **d** Quantifications of the width of EHD-printed filaments by using different inks with increasing PEO concentrations. **e**, **f** Effect of PEO concentration on the viscosity and surface tension of inks, respectively. **g**, **h** Light microscope images of EHD-printed 10- and 20-layer RGD-ALG/FIB/PEO hydrogel structures, respectively. All data are displayed as mean±standard deviation (SD). RGD: arginine–glycine–aspartic acid; ALG: alginate; FIB: fibrin

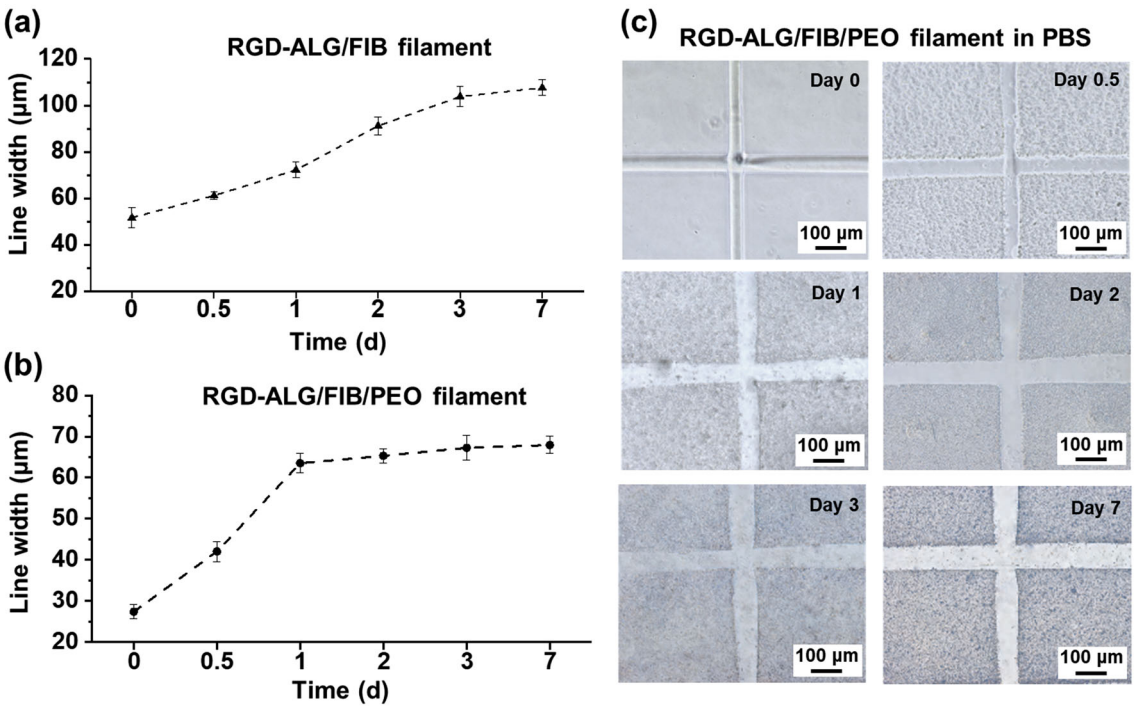

Fig. 4 The swelling behavior of electrohydrodynamic (EHD)-printed filaments. **a**, **b** Variations in the width of EHD-printed filaments by using inks without and with polyoxyethylene (PEO) addition after immersion in phosphate-buffered saline (PBS) solution up to one week. **c** Light microscope images of EHD-printed filaments after immersion in PBS solution for 7 days. All data are displayed as mean ± standard deviation (SD)

Subsequently, the swelling characteristics of EHD-printed scaffolds were investigated by measuring the diameter changes of single fibers when subjected to an aqueous environment over a period of 7 days (Figs. 4a–4c). The diameters of RGD-ALG/FIB and RGD-ALG/FIB/PEO fibers increased by approximately 120% and 160% compared to those before immersion, reaching a maximum of (107.6±3.9) μm and (67.9±2.1) μm after 7 days, respectively (Figs. 4a and 4b). This indicates that the incorporation of PEO can effectively constrain the diameter of printed fibers despite the exposure to an aqueous environment. Besides, RGD-ALG/FIB/PEO fibers reached equilibrium swelling on day 1, whereas RGD-ALG/FIB fibers reached this state on day 3, after which no change in morphology was observed until day 7. These results demonstrate that a reaction including sufficient crosslinking occurred instantly between the alginate-based ink and calcium ions inside the agarose substrate during fiber deposition, which led to the forming of a stable hydrogel construct that can maintain the desired structure in an aqueous environment. This construct allowed for the long-term culture of cells within the hydrogel filament in vitro with sustained patterning morphology.

In spite of the good biocompatibility of the optimized inks when using the extrusion bioprinting method above, the cell behavior was investigated using the EHD bioprinting strategy with RGD-ALG/FIB ink, PEO-incorporated RGD-ALG/FIB ink, and pure alginate ink as control. Cell-laden constructs with 10 layers were EHD-printed, as shown in Fig. 5. After 2 days of incubation, the C2C12s were found to be homogeneously distributed in the construct with spherical morphology in the EHD-printed scaffolds when using pure alginate bioink. In contrast, when using the RGD-ALG/FIB bioink, obviously improved cell spreading and extension could be observed along with a larger cell density. Further addition of PEO into the RGD-ALG/FIB bioink could lead to a high-resolution EHD-printed living scaffold with accurate single cell alignment following the deposition pattern of the fibers, as shown in Fig. 5c, in contrast to what was observed for the distribution of cells within large hydrogel filaments obtained by using PEO-free ink (≈ 50 μm, Fig. 5b) or through conventional extrusion-based bioprinting (≈ 200 μm Fig. 2g). Submicron features such as micro-/nanofibers and grooves are known to greatly guide cell alignment via contact stimuli and spatial constriction [15, 16]. No harmful effect on the cell activity was detected while using PEO as the viscosity enhancer, as shown in Fig. 5d, suggesting the overall safety of the ink. In addition, the functionalized bioink developed in this work could keep high cell viability and promote cell stretching in a cytoskeletal view. Figure 5e shows the

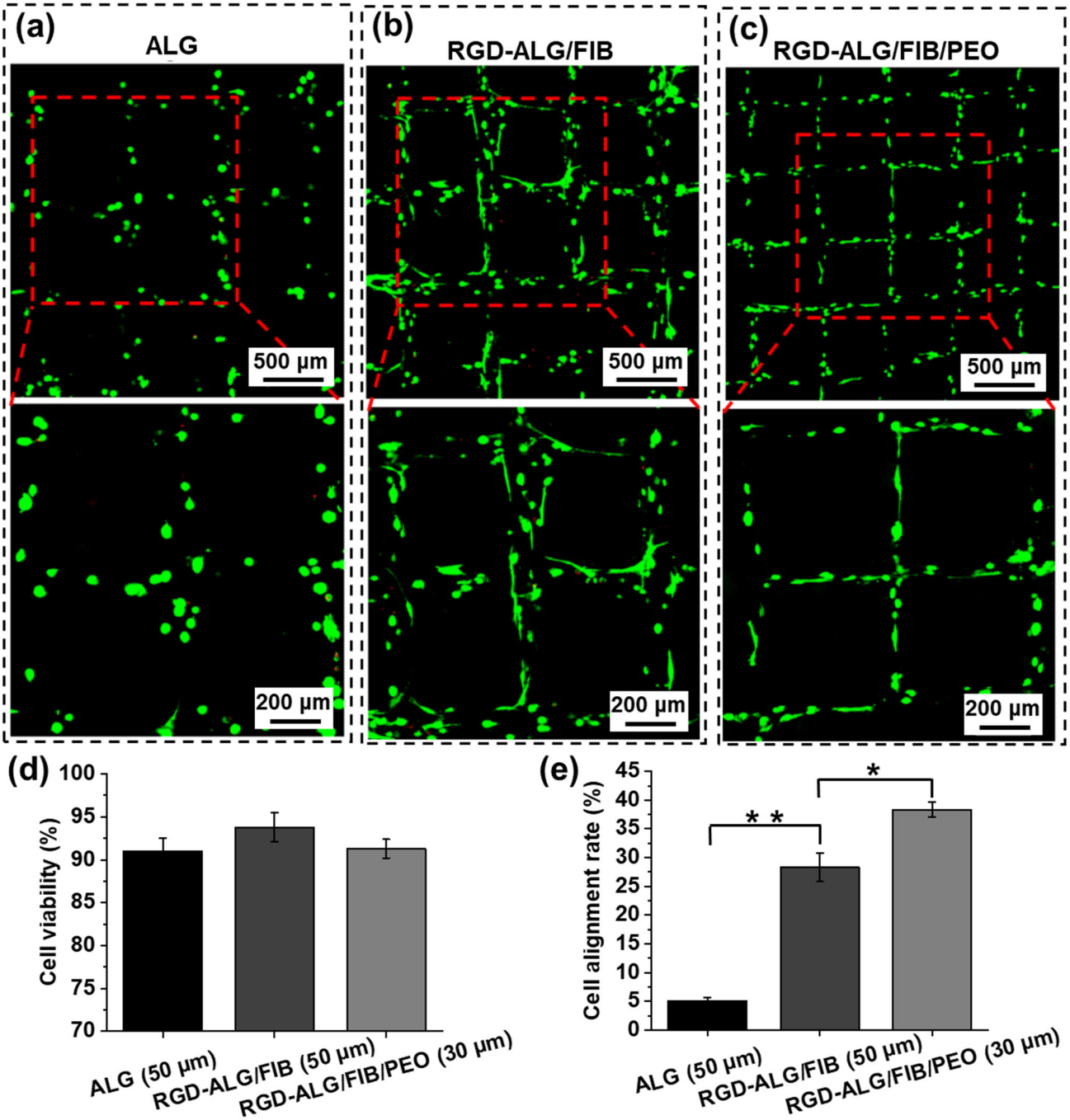

Fig. 5 The improvement of cellular alignment in living tissue constructs fabricated by different electrohydrodynamically printed alginate-based bioinks. **a–c** Fluorescent images of electrohydrodynamic (EHD)-printed 10-layer living constructs after 2 days of culture using pure alginate, RGD-ALG/FIB and RGD-ALG/FIB/PEO encapsulating C2C12s as bioinks, respectively. **d** Cell viability and **e** cell alignment rate of C2C12s inside EHD-printed 10-layer constructs by using different bioinks after 2 days of culture. All data are displayed as mean ± standard deviation (SD). $^{*}p<0.05$, $^{**}p<0.01$, as analyzed via one-way ANOVA. RGD: arginine–glycine–aspartic acid; ALG: alginate; FIB: fibrin; PEO: polyoxyethylene

quantitative statistics on cellular alignment based on confocal images, in which the aligned cells were defined as those having an absolute angle between 0° and 45° compared to the printing path [34]. It could be seen that the presence of fibrinogen and RGD peptides plays a significant role in boosting the spreading behavior of cells, and the cells were well-orientated along the direction of fiber deposition. Compared to conventional extrusion-based 3D bioprinting methods, EHD bioprinting enables the printing of submicrometer features without nozzle clogging or high-shear squeezing, as it can produce nanometer-sized jets from a large nozzle under the effect of high electric field [19, 45].

In order to better mimic the natural ECM with complex geometries and the layer-specific orientation of cells, "cell-laden" constructs with more complex geometries were designed and EHD-printed using the developed bioink. It can be seen from the light micrographs in Fig. 6a that cell-laden complex hexagonal pore structures could be obtained due to the precise patterning capabilities of the EHD bioprinting strategy. The multi-angle printed filaments could be accurately deposited and clearly visualized. In addition, EHD-printed C2C12s could sustain high viability as well as a structure-orientated alignment as observed by the live/dead staining results in Fig. 6b. After 5 days of culture, cells further elongated and occupied the entire length of the hydrogel lines, and the overall alignment was shown to be along the printing direction (Fig. 6c). Figure 6d shows a highly ordered cell nucleus along with the printing filaments. Previous research using the extrusion bioprinting method has reported a strain-induced cell alignment; that is, cells tended to align parallel to the strain direction during the printing process to attain maximum effective stiffness [46]. However, the overly large shear force applied on hydrogel struts during the extrusion process would cause cell death directly and has become the main critical issue of the extrusion bioprinting technique [47]. Given the above results, during the EHD bioprinting process of this study, bioinks with very low viscosity (<10 Pa·s) were used and a very small feeding rate of inks (80–300 μL/h) was applied, such that the shear stress was low enough (<8.49 kPa) to maintain good cell viability. Meanwhile, the low shear stress may not determine the cell growth direction; therefore, in this case, cells were printed by confining within thin filaments and thus tended to spread guided by geometry cues, which would result in the appropriate orientation. It should be noted that cells can possibly migrate out of the gel, while the thin fiber structure can still guide the directed growth of cells [48]. In this work, we covered a collagen layer on the top of the EHD-bioprinted constructs; in this case, the cells might tend to migrate out of the printed filaments, as shown in Fig. 6e. After 2 days of culture, the cell nuclei could arrange well according to the printing path (Fig. 6f), and cells could clearly spread in the desired orientation (Fig. 6g). In addition, cells can be aligned with the direction of electric field during the EHD printing process [49].

Overall, the EHD bioprinting strategy combining the functionalized alginate-based bioinks developed in this work was able to fabricate engineered constructs with high precision and controlled variation of cell alignment through the specified print path design, as well as keeping cell viability and spreading sufficient. Taken together, the approach used herein is capable of patterning hydrogel into 3D organized microfiber networks with high precision without damaging the encapsulated cells using the unique EHD bioprinting strategy. By adopting our functionalized alginate, remarkable cell alignment and spreading features can be successfully achieved for generating well-organized living microstructures.

Conclusions

In this work, we developed a functionalized alginate-based bioink for the microscale electrohydrodynamic bioprinting of living tissue constructs with improved cellular spreading and alignment. By the functionalization of alginate with RGD peptides and incorporation of fibrin and PEO, superior C2C12 viability and spreading behavior could be observed in the EHD-bioprinted cell-laden scaffolds from day 1 of culture. The addition of PEO could improve the printing accuracy significantly through reduced cell-laden fiber sizes (<30 μm), without scarifying the stability and biocompatibility of scaffolds. Angular changes at the multi-layer structures were printed and characterized to show high cellular orientation according to the printed microfibers. These outstanding features of the novel functionalized hydrogel bioinks and EHD process will make it possible to engineer microstructure scaffolds with promising physical and biological characteristics, to better resemble complex cellular microenvironments in nature.

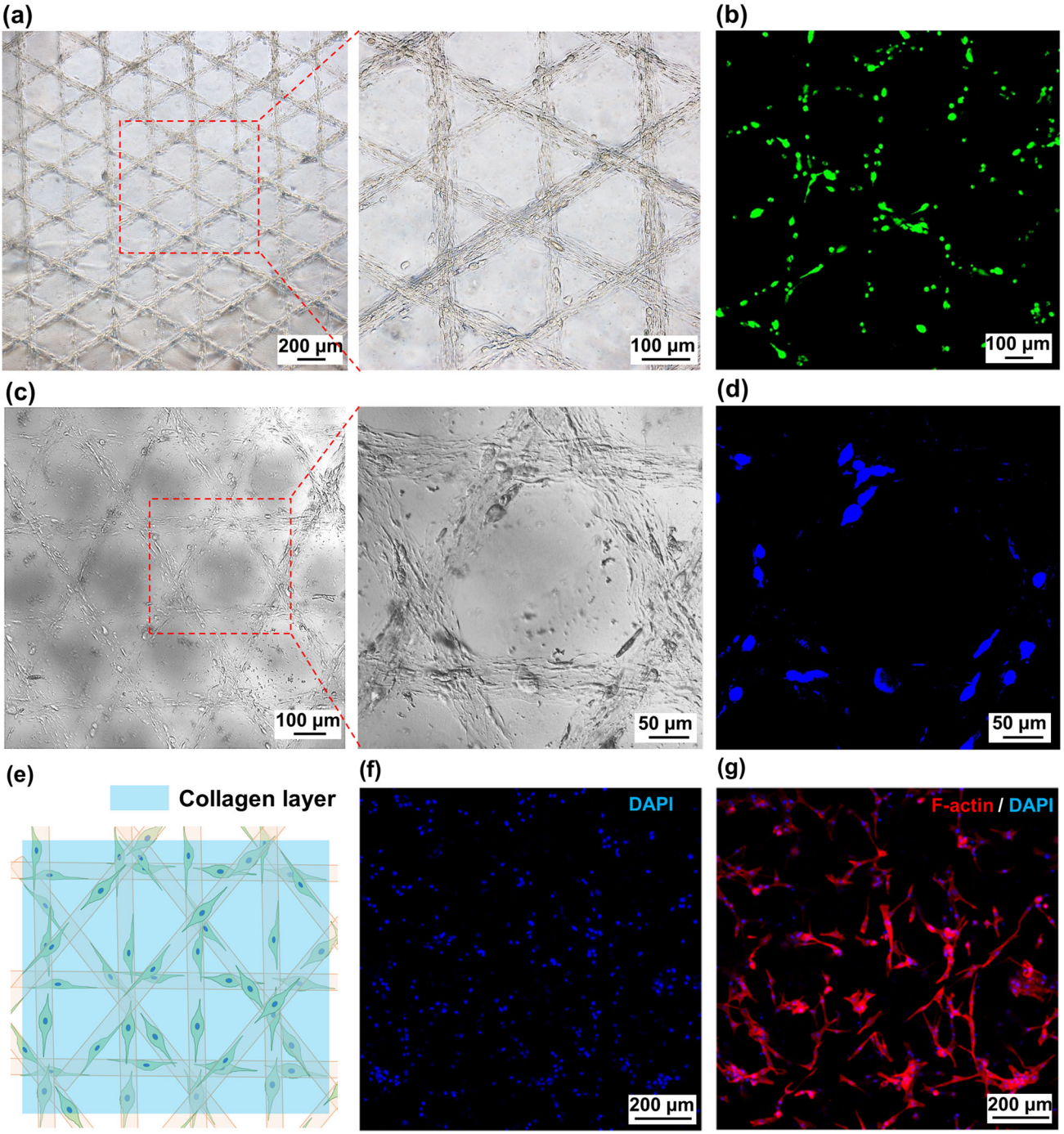

Fig. 6 **a** Light micrograph and its magnified image of electrohydrodynamic (EHD)-bioprinted layer-specific living constructs with 5 layers using RGD-ALG/FIB/PEO bioink after 1 day of culture. **b** Live/dead staining of EHD-printed layer-specific living tissue constructs with 5 layers using RGD-ALG/FIB/PEO bioink after 1 day of culture. **c** Light micrograph and its magnified image of EHD-bioprinted layer-specific living constructs made with 5 layers using RGD-ALG/FIB/PEO bioink after 5 days of culture. **d** Cell nucleus staining of EHD-bioprinted layer-specific living constructs made with 5 layers using RGD-ALG/FIB/PEO bioink after 5 days of culture. **e** Schematic diagram of the EHD-printed living constructs using RGD-ALG/FIB/PEO bioink covered by a collagen layer. **f**, **g** Cell nucleus and F-actin staining of the encapsulated cells after 2 days of culture. RGD: arginine–glycine–aspartic acid; ALG: alginate; FIB: fibrin; PEO: polyoxyethylene

Acknowledgements This work was financially supported by the National Key Research and Development Program of China (No. 2018YFA0703003), the National Natural Science Foundation of China (No. 52125501), the Key Research Project of Shaanxi Province (Nos. 2021LLRH-08, 2020GXLH-Y-021, and 2021GXLH-Z-028), the Youth Innovation Team of Shaanxi Universities and the Fundamental Research Funds for the Central Universities.

Author contributions ZNQ, YTW and AK were involved in the methodology and investigation; ZNQ contributed to the formal analysis; HZ assisted in writing—original draft; all authors participated in writing—review and editing; DCL and JKH contributed to the funding acquisition and supervision.

Declarations

Conflict of interest The authors declare that they have no conflict of interest.

Ethical approval This study does not contain any studies with human or animal subjects performed by any of the authors.

References

1. Vijayavenkataraman S, Yan WC, Lu WF et al (2018) 3D bioprinting of tissues and organs for regenerative medicine. Adv Drug Deliv Rev 132:296–332. https://doi.org/10.1016/j.addr.2018.07.004
2. Aljohani W, Ullah MW, Zhang X et al (2017) Bioprinting and its applications in tissue engineering and regenerative medicine. Int J Biol Macromol 107(Part A):261–275. https://doi.org/10.1016/j.ijbiomac.2017.08.171
3. Mota C, Camarero-Espinosa S, Baker MB et al (2020) Bioprinting: from tissue and organ development to in vitro models. Chem Rev 120(19):10547–10607. https://doi.org/10.1021/acs.chemrev.9b00789
4. Zhu H, Monavari M, Zheng K et al (2022) 3D bioprinting of multifunctional dynamic nanocomposite bioinks incorporating Cu-doped mesoporous bioactive glass nanoparticles for bone tissue engineering. Small 18(12):e2104996. https://doi.org/10.1002/smll.202104996
5. Li X, Liu B, Pei B et al (2020) Inkjet bioprinting of biomaterials. Chem Rev 120(19):10793–10833. https://doi.org/10.1021/acs.chemrev.0c00008
6. Dou C, Perez V, Qu J et al (2021) A state-of-the-art review of laser-assisted bioprinting and its future research trends. ChemBioEng Rev 8(5):517–534. https://doi.org/10.1002/cben.202000037
7. Heid S, Becker K, Byun J et al (2022) Bioprinting with bioactive alginate dialdehyde-gelatin (ADA-GEL) composite bioinks: time-dependent in-situ crosslinking via addition of calcium-silicate particles tunes in vitro stability of 3D bioprinted constructs. Bioprinting 26:e00200. https://doi.org/10.1016/j.bprint.2022.e00200
8. Moroni L, Burdick JA, Highley C et al (2018) Biofabrication strategies for 3D in vitro models and regenerative medicine. Nat Rev Mater 3(5):21–37. https://doi.org/10.1038/s41578-018-0006-y
9. Brassard JA, Lutolf MP (2019) Engineering stem cell self-organization to build better organoids. Cell Stem Cell 24(6):860–876. https://doi.org/10.1016/j.stem.2019.05.005
10. Xing J, Liu N, Xu N et al (2021) Engineering complex anisotropic scaffolds beyond simply uniaxial alignment for tissue engineering. Adv Funct Mater 32(15):2110676. https://doi.org/10.1002/adfm.202110676
11. Cui C, Yang C, Eidson N et al (2020) A highly reversible, dendrite-free lithium metal anode enabled by a lithium-fluoride-enriched interphase. Adv Mater 32(12):e1906427. https://doi.org/10.1002/adma.201906427
12. Choi SW, Choi Y, Kim J (2019) In situ magnetic alignment and cross-linking of injectable microparticles into centimeter-scale fibers for efficient myoblast alignment and in vivo fiber formation. Chem Mater 31(14):5181–5189. https://doi.org/10.1021/acs.chemmater.9b01276
13. Jana S, Levengood SK, Zhang M (2016) Anisotropic materials for skeletal-muscle-tissue engineering. Adv Mater 28(48):10588–10612. https://doi.org/10.1002/adma.201600240
14. Zhuang P, An J, Chua CK et al (2020) Bioprinting of 3D in vitro skeletal muscle models: a review. Mater Des 193:108794. https://doi.org/10.1016/j.matdes.2020.108794
15. Zhang Y, Zhang Z, Wang Y (2020) 3D myotube guidance on hierarchically organized anisotropic and conductive fibers for skeletal muscle tissue engineering. Mater Sci Eng C Mater Biol Appl 116:111070. https://doi.org/10.1016/j.msec.2020.111070
16. Charest JL, García AJ, King WP (2007) Myoblast alignment and differentiation on cell culture substrates with microscale topography and model chemistries. Biomaterials 28(13):2202–2210. https://doi.org/10.1016/j.biomaterials.2007.01.020
17. Mao M, He J, Li Z et al (2020) Multi-directional cellular alignment in 3D guided by electrohydrodynamically-printed microlattices. Acta Biomater 101:141–151. https://doi.org/10.1016/j.actbio.2019.10.028
18. Jing L, Sun J, Liu H et al (2021) Using plant proteins to develop composite scaffolds for cell culture applications. Int J Bioprint 7(1):298. https://doi.org/10.18063/ijb.v7i1.298
19. Zhang B, He J, Li X et al (2016) Micro/nanoscale electrohydrodynamic printing: from 2D to 3D. Nanoscale 8(34):15376–15388. https://doi.org/10.1039/c6nr04106j
20. Ye W, Xie C, Liu Y et al (2021) 3D printed high-resolution scaffold with hydrogel microfibers for providing excellent biocompatibility. J Biomater Appl 35(6):633–642. https://doi.org/10.1177/0885328220962606
21. Gao Q, Xie C, Wang P et al (2020) 3D printed multi-scale scaffolds with ultrafine fibers for providing excellent biocompatibility. Mater Sci Eng C Mater Biol Appl 107:110269. https://doi.org/10.1016/j.msec.2019.110269
22. Wang C, Xu Y, Xia J et al (2021) Multi-scale hierarchical scaffolds with aligned micro-fibers for promoting cell alignment. Biomed Mater 16(4):045047. https://doi.org/10.1088/1748-605X/ac0a90
23. Hu S, Meng Z, Zhou J et al (2022) Enhanced attachment and collagen type I deposition of MC3T3-E1 cells via electrohydrodynamic printed sub-microscale fibrous architectures. Int J Bioprint 8(2):514. https://doi.org/10.18063/ijb.v8i2.514
24. He J, Hao G, Meng Z et al (2021) Expanding melt-based electrohydrodynamic printing of highly-ordered microfibrous architectures to cm-height via in situ charge neutralization. Adv Mater Technol 7(7):2101197. https://doi.org/10.1002/admt.202101197
25. He J, Zhao X, Chang J et al (2017) Microscale electrohydrodynamic cell printing with high viability. Small 13(47):1702626. https://doi.org/10.1002/smll.201702626
26. Sampson SL, Saraiva L, Gustafsson K (2014) Cell electrospinning: an in vitro and in vivo study. Small 10(1):78–82. https://doi.org/10.1002/smll.201300804
27. Yeo M, Kim G (2020) Micro/nano-hierarchical scaffold fabricated using a cell electrospinning/3D printing process for co-culturing myoblasts and HUVECs to induce myoblast alignment and differentiation. Acta Biomater 107:102–114. https://doi.org/10.1016/j.actbio.2020.02.042
28. Yeo M, Ha J, Lee H et al (2016) Fabrication of hASCs-laden structures using extrusion-based cell printing supplemented with an electric field. Acta Biomater 38:33–43. https://doi.org/10.1016/j.actbio.2016.04.017

29. Yeo M, Kim GH (2018) Anisotropically aligned cell-laden nanofibrous bundle fabricated via cell electrospinning to regenerate skeletal muscle tissue. Small 14(48):e1803491. https://doi.org/10.1002/smll.201803491
30. Castilho M, Levato R, Bernal PN et al (2021) Hydrogel-based bioinks for cell electrowriting of well-organized living structures with micrometer-scale resolution. Biomacromol 22(2):855–866. https://doi.org/10.1021/acs.biomac.0c01577
31. Galliger Z, Vogt CD, Panoskaltsis-Mortari A (2019) 3D bioprinting for lungs and hollow organs. Transl Res 211:19–34. https://doi.org/10.1016/j.trsl.2019.05.001
32. Ballester-Beltrán J, Lebourg M, Rico P et al (2012) Dorsal and ventral stimuli in cell-material interactions: effect on cell morphology. Biointerphases 7:39. https://doi.org/10.1007/s13758-012-0039-5
33. Bauer A, Gu L, Kwee B et al (2017) Hydrogel substrate stress-relaxation regulates the spreading and proliferation of mouse myoblasts. Acta Biomater 62:82–90. https://doi.org/10.1016/j.actbio.2017.08.041
34. Vion AC, Perovic T, Petit C et al (2021) Endothelial cell orientation and polarity are controlled by shear stress and VEGF through distinct signaling pathways. Front Physiol 11:623769. https://doi.org/10.3389/FPHYS.2020.623769
35. Finch DA, Ralph B, Gilding K (1997) Determination of the cation content of alginate thin films by *FT*i.r. spectroscopy. Polymer 38(1):43–51. https://doi.org/10.1016/S0032-3861(96)00458-2
36. Tenchurin TK, Pavlovsky MM, Shepelev AD et al (2019) Modification of non-woven materials based on sodium alginate for tissue-engineering. J Phys Conf Ser 1347:012072. https://doi.org/10.1088/1742-6596/1347/1/012072
37. Sun J, Wei D, Yang K et al (2017) The development of cell-initiated degradable hydrogel based on methacrylated alginate applicable to multiple microfabrication technologies. J Mater Chem B 5(40):8060–8069. https://doi.org/10.1039/c7tb01458a
38. Du J, Zhou C, Xia Q et al (2022) The effect of fibrin on rheological behavior, gelling properties and microstructure of myofibrillar proteins. LWT 153:112457. https://doi.org/10.1016/j.lwt.2021.112457
39. Vicar T, Balvan J, Jaros J (2019) Cell segmentation methods for label-free contrast microscopy: review and comprehensive comparison. BMC Bioinform 20:360. https://doi.org/10.1186/s12859-019-2880-8
40. Indana D, Agarwal P, Bhutani N et al (2021) Viscoelasticity and adhesion signaling in biomaterials control human pluripotent stem cell morphogenesis in 3D culture. Adv Mater 33(43):e2101966. https://doi.org/10.1002/adma.202101966
41. Bidarra SJ, Barrias CC, Granja PL (2014) Injectable alginate hydrogels for cell delivery in tissue engineering. Acta Biomater 10(4):1646–1662. https://doi.org/10.1016/j.actbio.2013.12.006
42. Tiwari SK, Venkatraman SS (2012) Importance of viscosity parameters in electrospinning: of monolithic and core–shell fibers. Mater Sci Eng C 32(5):1037–1042. https://doi.org/10.1016/j.msec.2012.02.019
43. Kim MW, Cao BH (1993) Additional reduction of surface tension of aqueous polyethylene oxide (PEO) solution at high polymer concentration. EPL 24(3):229–234. https://doi.org/10.1209/0295-5075/24/3/012
44. Liashenko I, Rosell-Llompart J, Cabot A (2020) Ultrafast 3D printing with submicrometer features using electrostatic jet deflection. Nat Commun 11(1):753. https://doi.org/10.1038/s41467-020-14557-w
45. Zhao X, He J, Xu F et al (2016) Electrohydrodynamic printing: a potential tool for high-resolution hydrogel/cell patterning. Virtual Phys Prototyp 11(1):57–63. https://doi.org/10.1080/17452759.2016.1139378
46. Lee JM, Yeong WY (2020) Engineering macroscale cell alignment through coordinated toolpath design using support-assisted 3D bioprinting. J R Soc Interface 17(168):20200294. https://doi.org/10.1098/rsif.2020.0294
47. Schwab A, Levato R, D'Este M (2020) Printability and shape fidelity of bioinks in 3D bioprinting. Chem Rev 120(19):11028–11055. https://doi.org/10.1021/acs.chemrev.0c00084
48. Aubin H, Nichol JW, Hutson CB et al (2010) Directed 3D cell alignment and elongation in microengineered hydrogels. Biomaterials 31(27):6941–6951. https://doi.org/10.1016/j.biomaterials.2010.05.056
49. Yang GH, Kim W, Kim J et al (2021) A skeleton muscle model using GelMA-based cell-aligned bioink processed with an electric-field assisted 3D/4D bioprinting. Theranostics 11(1):48–63. https://doi.org/10.7150/THNO.50794